

Energy bands, electronic properties, and magnetic ordering of CrB_2

S. H. Liu*

*Ames Laboratory, United States Energy Research and Development Administration
and Department of Physics, Iowa State University, Ames, Iowa 50010*

L. Kopp

*Ames Laboratory, United States Energy Research and Development Administration
and Department of Chemistry, Iowa State University, Ames, Iowa 50010*

W. B. England

Chemistry Division, Argonne National Laboratory, Argonne, Illinois 60439

H. W. Myron†

Magnetic Theory Group, Department of Physics, Northwestern University, Evanston, Illinois 60201

(Received 11 February 1974; revised manuscript received 8 July 1974)

The energy bands of the compound CrB_2 have been calculated by using the Korringa-Kohn-Rostoker method in the muffin-tin-potential approximation. The bands near the Fermi level have mostly Cr d character, and one of the bands gives rise to a very flat piece of Fermi surface perpendicular to the hexagonal axis. We propose that this piece of Fermi surface stabilizes a spin-density-wave state which manifests itself as antiferromagnetic ordering of the compound below 85 K. We also interpret the excess specific heat and electronic-spin susceptibility as due to exchange enhancement.

INTRODUCTION

Barnes and his collaborators established by NMR measurements that the compound CrB_2 orders antiferromagnetically below 85 K.^{1,2} The compound is metallic, and furthermore, the temperature dependence of the resonance amplitude resembles that of Cr and its alloys rather than that of a classical Heisenberg-type antiferromagnet. Therefore, Barnes *et al.* concluded that CrB_2 is an itinerant-electron antiferromagnet like Cr itself.

Castaing and his co-workers studied a series of transition-metal diborides: ScB_2 , TiB_2 , VB_2 , and CrB_2 .³⁻⁶ They measured the specific heat and electronic-spin susceptibility of these compounds and the elastic-neutron-diffraction pattern of CrB_2 . It was found that CrB_2 has an electronic-spin susceptibility which is an order of magnitude higher than that of the other diborides and that its specific heat is also a factor of 2 or more higher. The neutron-diffraction pattern of a powder sample of CrB_2 shows evidence of magnetic satellites at helium temperature. These results demonstrate that there is a large exchange-enhancement effect in CrB_2 , one much larger than that in the other diborides.

As in the case of pure transition metals, large exchange enhancement does not necessarily lead to antiferromagnetic ordering. As was first shown by Lomer,⁷ a particular Fermi-surface geometry, commonly called "nesting Fermi surfaces," is needed to stabilize a spin-density-wave state. We calculated the energy bands and Fermi surface of CrB_2 in order to determine whether the Lomer model also applies to this compound.

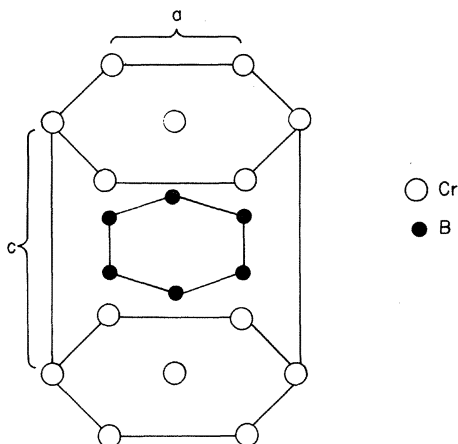
An augmented-plane-wave (APW) band calcula-

tion for CrB_2 was done previously by McAlister *et al.*⁸ The calculation was done on too crude a mesh for the purpose of Fermi-surface study, but it was used with considerable success to compute densities of states and soft-x-ray photoemission spectra for a series of $3d$ -metal diborides.

We chose to perform the calculation by using the Korringa-Kohn-Rostoker (KKR) method,^{9,10} for reasons reviewed in a recent publication whose authors included two of us.¹¹ Briefly speaking, when applied to compounds the APW method requires the calculation and diagonalization of a very large matrix in order to get accurate eigenvalues. In practice one is limited to calculating the energy bands at high-symmetry points, and one must rely on interpolation schemes to generate bands at general points in the Brillouin zone. The KKR method, on the other hand, involves a much smaller matrix, and there is no need to use any interpolation scheme to determine the band structure throughout the Brillouin zone. The disadvantage of the KKR method is that it takes longer to compute the matrix elements, although recent work by Williams *et al.* has overcome this problem for pure metals.¹² We were unable to apply their innovation because it requires a larger memory capacity than we have available.

DETAILS OF CALCULATIONS

The crystal structure of CrB_2 is designated $C32^{13}$ and is depicted in Fig. 1. It is simply a hexagonal lattice in which closest-packed Cr layers alternate with graphitelike B layers. Using the primitive lattice translation vectors as the basis, the positions of the atoms in the unit cell may be indicated by choosing the coordinates (0, 0, 0) for

FIG. 1. Crystal structure of CrB_2 .

Cr and $(\frac{1}{3}, \frac{2}{3}, \frac{1}{2})$, $(\frac{2}{3}, \frac{1}{3}, \frac{1}{2})$ for B. The lattice parameters a and c have the values 2.969 and 3.066 Å, respectively.¹³ The Cr-B and B-B bond lengths are calculated to be 2.300 and 1.714 Å, respectively.

The muffin-tin (MT) radii were determined by the following observations. If the MT radius of Cr is chosen to be one-half of a , or 1.484 Å, and if the sum of the Cr and B MT radii is set equal to the Cr-B bond length, fixing the B MT radius at 0.816 Å, then none of the muffin-tin spheres overlap. Moreover, they either touch or almost touch along all bonds, and about 80% of the unit cell volume lies within them. These radii are close to the Bragg-Slater atomic radii, 1.40 Å for Cr and 0.85 Å for B, which are quite successful in reproducing observed interatomic distances and which correlate well with computed radii of the maximum radial charge density in the outermost shells of the atoms, 1.45 Å for Cr 4s and 0.78 Å for B 2p.¹⁴ The choice of MT radii is not crucial, as previous calculations on compounds have shown the energy bands to be quite insensitive to small changes (~4%) in them.^{11,15}

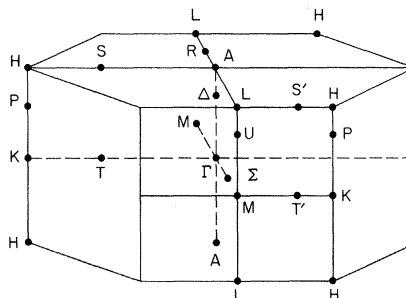
The crystal potential was constructed by the *ad hoc* method of Mattheiss¹⁶ using the neutral-atom charge densities.¹⁷ The atomic configurations are Cr: $3d^5 4s^1$ and B: $2s^2 2p^1$. The full Slater exchange potential was assumed.¹⁸ The average potential in the interstitial region, which was found to be -2.041 Ry, was taken as the reference point for the muffin-tin potential. Since the crystal is very closely packed, we do not expect the non-muffin-tin part of the interstitial potential to be important. This crystal potential is the same as that used by McAlister *et al.*⁸

The calculation is not self-consistent. This might seem to call our results into question, especially since we find a significant shift from the

initial charge density. Our cause for confidence comes from the following work. Snow and Waber,¹⁹ Connolly,²⁰ Papaconstantopoulos *et al.*,²¹ and Anderson *et al.*²² found from their respective self-consistent calculations on Cu, Ni, V, and Nb that the interplay of configuration and exchange led to astonishing over-all agreement between non-self-consistent results using full Slater ($\alpha=1$) exchange and self-consistent results using less than full Slater exchange. Recent calculations by Walch and Ellis on MgO,²³ Myron and Freeman on TiS_2 ,^{24,25} and Moruzzi *et al.* on β -brass (CuZn),¹⁵ support the same conclusion for compounds, even when there is evidence of charge transfer.

The s , p , and d orbitals of all atoms in the unit cell were included in the calculation, so the order of the KKR matrix was 27. The Ham and Segall²⁶⁻²⁸ method was used to evaluate the matrix elements. The Ewald parameter was chosen to be 0.6, and the real and reciprocal lattice sums were truncated to 21 and 59 terms, respectively. The matrix elements were calculated within an accuracy of 10^{-5} Ry⁻¹. The energy eigenvalues were calculated on a mesh of six equally spaced layers from Γ to A in the Brillouin zone (Fig. 2) with 21 points uniformly distributed in each $\frac{1}{12}$ sector of the basal plane in each layer. Over an energy range from 0 to 1.5 Ry we found from 9 to 12 eigenvalues for each wave vector. The eigenvalues were evaluated by iteration to an accuracy of 0.002 Ry. The resulting energy bands are plotted in Fig. 3.

For calculation of the density of states and the Fermi surface the coarse mesh for finding energy eigenvalues was made finer by interpolation using the method of "spline fits."²⁹ This method does not involve a parametric fitting of the calculated points to some assumed functional form. Such schemes, as are the QUAD and Slater-Koster methods, are especially useful on a coarser mesh where the details of the band structure are not clearly reflected in the calculated points. Starting from a less coarse mesh it becomes important for a fitting procedure to reproduce the smoothness of the energy bands without introducing additional errors

FIG. 2. Brillouin zone of CrB_2 .

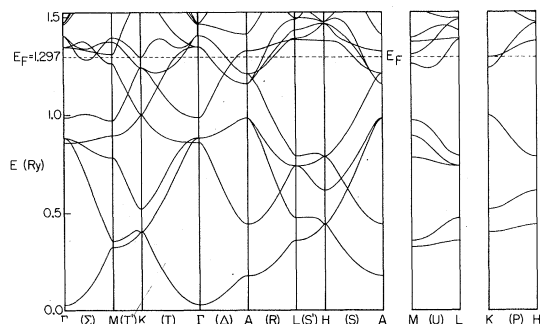


FIG. 3. Energy bands of CrB_2 along the symmetry axes.

at the calculated points. Spline interpolation is the standard way to achieve this result. It essentially makes a piecewise cubic fit which ensures continuity of the values, slopes, and curvatures at the points calculated.

To obtain the density of states we interpolated the calculated bands to a finer mesh of 187 000 points in the Brillouin zone, and counted in energy increments of 0.01 Ry. The integrated density of states was calculated by counting in a finer energy increment of 0.001 Ry. The results are shown in Fig. 4, where the scale for $N(E)$ is on the left and that for the integral, $\int N(E) dE$, is on the right. The bands must accommodate 12 electrons, 3 from each boron and 6 from Cr. This fixes the Fermi level at 1.297 Ry. The density of states has two peaks: a narrow peak just above the Fermi level due to the narrow Cr d bands, and a broader peak at 0.8 Ry from mixed Cr p, d and B p states. The result of McAlister *et al.* has the same general features.⁸

The Fermi surface was determined by first interpolating the bands to a mesh of 1700 points in the Brillouin zone and then scanning between pairs

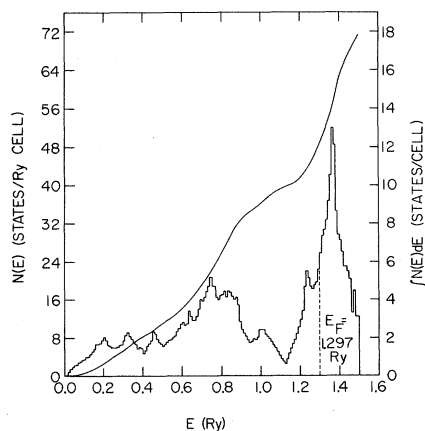


FIG. 4. Density of states (histogram) and integrated density of states (smooth curve) of CrB_2 .

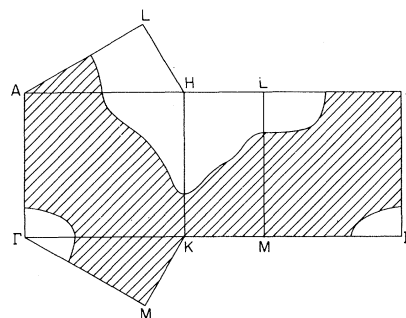


FIG. 5. 6th-band Fermi surface of CrB_2 .

of nearest-neighbor mesh points. If a band was found to cross the Fermi energy between two of these points, the band was fitted to a quadratic function of the wave vector, and the root of $E(\vec{k}) = E_F$ was determined analytically. Numbering the bands in ascending order of energy, bands 6, 7, and 8 cross the Fermi level. The Fermi surface of band 6 consists of a hole pocket centered around Γ and a large multiply connected piece as shown in Fig. 5. The Fermi surface of band 7 consists of two electron pockets around K and A as shown in Fig. 6. Band 8 contributes a small electron pocket around A with a shape very similar to that of band 7 at A .

We also studied the wave functions of the occupied bands to determine the character of the electronic states at the Fermi level and to gain some notion about the charge redistribution accompanying formation of the compound. The total populations of the three bands of CrB_2 which cross the Fermi level and their density of states populations at the Fermi level are presented in Table I. Of particular interest is the nearly pure Cr d character of the highest occupied states: of the 20.9 states/(Ry cell) at the Fermi level, 18.0 states/(Ry cell) are Cr d . Table II presents the distribution of the 12 valence electrons in the unit cell according to the same geometrical partitioning of the crystal used to calculate the energy bands. These numbers indicate a shift relative to the superposed

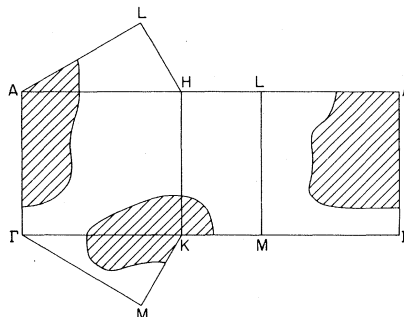


FIG. 6. 7th-band Fermi surface of CrB_2 .

TABLE I. Density-of-states population at E_F and total band population of the three partially filled bands of CrB_2 . The B contributions include both B atoms.

Band	6	7	8	Total
Cr <i>s</i>	0.07	0.08	0.01	0.16
<i>p</i>	0.53	0.80	0.06	1.39
<i>d</i>	6.37	10.48	1.16	18.01
B <i>s</i>	0.05	0.08	0.01	0.14
<i>p</i>	0.28	0.76	0.16	1.20
Total	7.3	12.2	1.4	20.9
Total band population	1.48	0.47	0.05	2.00

neutral-atom charge density of electrons from the region about B to the region about Cr on formation of CrB_2 . This shift is in the opposite direction from that found by McAlister *et al.*⁸ The small number of points in the Brillouin zone at which their calculation was performed could account for this discrepancy. Of perhaps more concern is that this shift is opposite to that anticipated by chemical intuition. While arguments have been advanced favoring either direction of the charge redistribution in the borides,^{30,31} we hesitate to make any interpretation of this result before performing a self-consistent calculation. The shift itself is evidence of the lack of self-consistency in this work and, since wave functions are more sensitive to self-consistency than are energies, we now are engaged in making this improvement.

ELECTRONIC PROPERTIES

The paramagnetic susceptibility of CrB_2 is only slightly temperature dependent, and above the Néel temperature it is approximately 600×10^{-6} emu/mole.³ Using the calculated density of states at the Fermi level, $N(E_F) = 20.9$ states/(Ry cell), we find the unenhanced Pauli susceptibility to be 58×10^{-6} emu/mole. The discrepancy between this and the experimental value is considerable. The recent neutron form factor measurement on paramagnetic Cr revealed that the total susceptibility, 160×10^{-6} emu/mole, comes 60% from orbital and 40% from spin contributions.³² If we make the crude estimate that the orbital susceptibility of Cr in CrB_2 equals that of Cr in the pure metal, namely 100×10^{-6} emu/mole, then the spin contribution to the susceptibility of CrB_2 would be about 500×10^{-6} emu/mole. This, together with the theoretical estimate, gives an exceedingly large enhancement factor³³ of 8.7.

From the measured specific heat Castaing estimated the effective density of states at the Fermi level to be $N^*(E_F) = 79$ states/(Ry cell),⁵ which is

a factor of 3.8 higher than our calculated value. Although the calculation of the density of states has some serious shortcomings, most notably the lack of self-consistency, the use of interpolation, and the neglect of the electron-phonon interaction, we doubt that correcting all of these could significantly reduce the discrepancy between theory and experiment. There must then be a large enhancement factor due to spin fluctuations.³³ Indeed, one can estimate from the formulas in Ref. 33 that a susceptibility enhancement factor of 8.7 is consistent with a specific-heat enhancement factor of 2.3, which is a sizable fraction of 3.8.

We may use the rigid-band model and the energy bands of CrB_2 to estimate the electronic properties of ScB_2 , TiB_2 , and VB_2 by simply making an appropriate shift of the Fermi level. This was also done in Ref. 8, and Fig. 7 shows our results together with those of McAlister *et al.*⁸ and the experimental results.⁶ There is good agreement between the two calculations, and good agreement with experiment except for CrB_2 . We have already discussed the exchange enhancement effect in CrB_2 . It turns out that when the Fermi level is shifted downward, the partially filled bands very rapidly lose their *d* character. This is the reason why the enhancement factor due to spin fluctuations reduces to almost unity for the other diborides.

The three bands near the Fermi level have exceedingly small boron *s* character in their wave functions, no more than 1%. This means that, in spite of the large spin susceptibility, the spin polarization can not reach the B nuclei effectively to produce a Knight shift. The measured Knight shift is in accord with this picture.^{1,6}

MAGNETIC ORDERING

The Lomer model for itinerant antiferromagnetism requires two sheets of Fermi surface which are nearly parallel.⁷ A study of the Fermi surface of CrB_2 reveals a rather large and flat piece of Fermi surface around the ΓA axis due to the 7th band (see Fig. 6). This piece may nest with its counterpart in the negative momentum region of the Brillouin zone. In Fig. 8 the 7th-band Fermi surface is replotted to show this nesting feature. The

TABLE II. Geometrical partitioning of the valence electrons of CrB_2 .

Number of valence electrons	Cr	B	CrB_2
For the free neutral atoms	6	3	12
Inside the MT spheres for the free neutral atoms	5.0	1.1	7.2
Inside the MT spheres for the superposed neutral atoms	7.2	1.4	10.0
Inside the MT spheres for the occupied crystalline states.	8.4	0.6	9.6

separation between the two pieces varies between Q_1 and Q_2 . There is another extremum dimension, Q_3 , but there is no distinct nesting feature associated with it.

A quantitative way to demonstrate the nesting of Fermi surfaces is to calculate the generalized susceptibility function.³⁴⁻³⁷ The function is defined as

$$\chi(\vec{Q}) = \sum_{\vec{k}} \frac{f_{\vec{k}}(1-f_{\vec{k}+\vec{Q}})}{E_{\vec{k}+\vec{Q}} - E_{\vec{k}}}, \quad (1)$$

where $f_{\vec{k}}$ is the Fermi distribution function. For more than one band one also sums over band indices for the two states $E_{n\vec{k}}$ and $E_{n',\vec{k}+\vec{Q}}$. This definition of $\chi(Q)$ leaves out the generalized oscillator-strength matrix elements between the Bloch states.³⁷ Gupta and Sinha showed for Cr that inclusion of these matrix elements affects the magnitude but not the position of the calculated peak in the susceptibility. We performed this calculation for the 7th band with Q along the c axis of the crystal. The band was first interpolated to a fine mesh of 1 000 000 points in the Brillouin zone, and then the sum was explicitly carried out for every pair of states such that $E_{\vec{k}}$ is below the Fermi level and $E_{\vec{k}+\vec{Q}}$ above. If the two energies differed by less than 0.0001 Ry the pair was discarded in accordance with the principal value integration. The result is shown in Fig. 9.

If the nesting Fermi surfaces were planes or exactly parallel surfaces, there would be a logarithmic singularity at that Q which is the separation between the pieces. In the present case we see a broad but distinct peak between Q_1 and Q_2 . The wave vector of the spin-density wave is determined by the maximum of the $\chi(Q)$ curve. Thus, the predicted wave vector is $Q_0 = 0.26 \tau_c$, where $\tau_c = 2\pi/c$.

Castaing reported an elastic neutron experiment

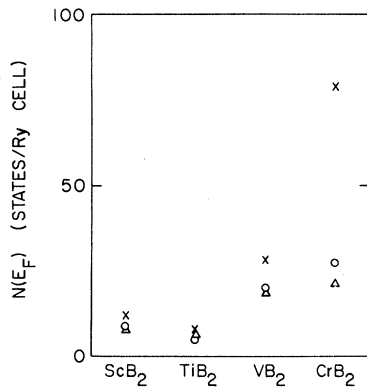


FIG. 7. Theoretical vs experimental density of states at the Fermi level for ScB_2 , TiB_2 , VB_2 and CrB_2 . The circles are from Ref. 8, the triangles are our results, and the crosses are deduced from experimental specific heats.

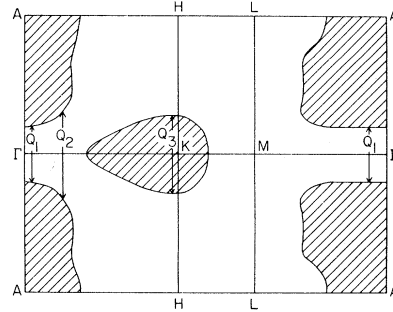


FIG. 8. 7th-band Fermi surface showing nesting features.

on a powdered sample of CrB_2 at helium temperature.⁶ He observed three very weak peaks that are probably of magnetic origin. Their positions, converted into units of τ_c , are 0.58, 0.74, and 1.15. The peak expected at Q_0 lies buried beneath the Bragg peak and cannot be detected, but the strongest magnetic satellite at $0.74 \tau_c$ may be interpreted as $\tau_c - Q_0$. Unfortunately the satellite then expected at $\tau_c + Q_0$ falls beyond the range of the experiment. The other two peaks are so weak they may be untrustworthy, or they may be higher harmonics of Q_0 .

The theory of itinerant antiferromagnetism shows that a band gap, 2Δ , develops when the system orders.³⁸ The low-temperature value of the gap is related to the Néel temperature, T_N , by $2\Delta = 3.5kT_N$. We find from this relation $2\Delta = 0.026 \text{ eV}$. The band gap is in turn related to the amplitude of the spin-density wave, or the average magnetization σ by $\Delta = \sigma V$, where V is the effective exchange potential. We can estimate from expression of the enhancement factor as $[1 - N(E_F)V]^{-1} = 8.7$, where $N(E_F) = 20.9$ is the calculated density of states, that

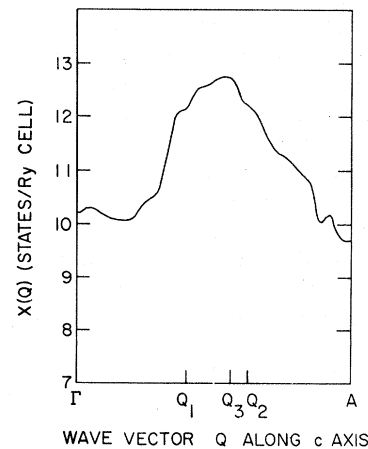


FIG. 9. Generalized susceptibility of CrB_2 along the c axis of the crystal.

$V = 1.2$ eV. This gives an estimate of the magnetization $\sigma = 0.01\mu_B$. This value is consistent with the experimental estimate of $0.02 - 0.1\mu_B$.⁶

Finally, as a consequence of ordering, we can use the relation³⁸ $kT_N = 1.14D e^{-1/NV}$ to obtain another estimate of the exchange energy V . The quantity D is half of the band-7 bandwidth (~ 0.1 Ry) and N is the density of states per spin contributed by band 7 to the nesting Fermi surfaces. Assuming that about $\frac{1}{3}$ of the band-7 Fermi surfaces nest, we obtain $V \cong 1.35$ eV, in very close agreement with our previous estimate of 1.2 eV.

In conclusion, we have shown through a band calculation that CrB_2 has the required band struc-

ture for an itinerant antiferromagnet. The band data correlate well with the electronic properties of CrB_2 if we include the exchange enhancement effect in the Cr d bands. Using a rigid band model we can also explain the systematic behavior of the electronic properties of the diborides of Sc, Ti and V.

ACKNOWLEDGMENTS

The authors are indebted to Professor R. G. Barnes for suggesting the investigation, and to Professors S. K. Sinha and C. Stassis for helpful discussions.

*Work done at Ames Laboratory—United States Atomic Energy Commission, Iowa State University, Ames, Iowa 50010.

†Supported by National Science Foundation through Northwestern University Materials Research Center and by Air Force Office of Scientific Research.

¹R. G. Barnes and R. G. Creel, *Phys. Lett. A* **29**, 203 (1969).

²R. J. Schoenberger and R. G. Barnes, *AIP Conf. Proc.* **5**, 392 (1971).

³J. Castaing, P. Costa, M. Heritier, and P. Lederer, *J. Phys. Chem. Solids* **33**, 533 (1972).

⁴J. Castaing, J. Danan, and M. Rieux, *Solid State Commun.* **10**, 563 (1972).

⁵J. Castaing, R. Caudron, G. Toupance, and P. Costa, *Solid State Commun.* **7**, 1453 (1969).

⁶J. Castaing, thesis (University of Paris, 1971) (unpublished).

⁷W. M. Lomer, *Proc. Phys. Soc. Lond.* **80**, 489 (1962).

⁸A. J. McAlister, J. R. Cuthill, M. L. Williams, and R. C. Dobbyn, in *Proceedings of the International Symposium on X-ray Spectra and Electronic Structure of Matter, Munich, 1972* (to be published).

⁹J. Korringa, *Physica (Utr.)* **13**, 392 (1947).

¹⁰W. Kohn and N. Rostoker, *Phys. Rev.* **94**, 1111 (1954).

¹¹H. W. Myron, R. P. Gupta, and S. H. Liu, *Phys. Rev. B* **8**, 1292 (1973).

¹²A. R. Williams, J. F. Janak, and V. L. Moruzzi, *Phys. Rev. B* **6**, 4509 (1972).

¹³W. B. Pearson, *A Handbook of Lattice Spacings and Structures of Metals and Alloys* (Pergamon, New York, 1958).

¹⁴J. C. Slater, *Quantum Theory of Molecules and Solids* (McGraw-Hill, New York, 1965), Vol. 2, pp. 101–108.

¹⁵V. L. Moruzzi, A. R. Williams, and J. F. Janak, *Phys. Rev. B* **9**, 3316 (1974).

¹⁶L. F. Mattheiss, *Phys. Rev.* **133**, A1399 (1964).

¹⁷F. Herman and S. Skillman, *Atomic Structure Calculations* (Prentice Hall, Englewood Cliffs, N. J., 1963).

¹⁸J. C. Slater, *Phys. Rev.* **81**, 385 (1951).

¹⁹E. C. Snow and J. T. Waber, *Phys. Rev.* **157**, 570 (1967).

²⁰J. W. D. Connolly, *Phys. Rev.* **159**, 415 (1967).

²¹D. A. Papaconstantopoulos, J. R. Anderson, and J. W. McCaffrey, *Phys. Rev. B* **5**, 1214 (1972).

²²J. R. Anderson, D. A. Papaconstantopoulos, J. W. McCaffrey, and J. E. Schirber, *Phys. Rev. B* **7**, 5115 (1973).

²³P. F. Walch and D. E. Ellis, *Phys. Rev. B* **8**, 5920 (1973).

²⁴H. W. Myron and A. J. Freeman, *Phys. Rev. B* **9**, 481 (1974).

²⁵H. W. Myron (private communication).

²⁶B. Segall, *Phys. Rev.* **105**, 108 (1957).

²⁷F. S. Ham and B. Segall, *Phys. Rev.* **124**, 1786 (1961).

²⁸B. Segall and F. S. Ham, *Methods Comput. Phys.* **8**, 251 (1968).

²⁹R. H. Pennington, *Introductory Computer Methods and Numerical Analysis* (MacMillan, New York, 1965).

³⁰R. B. Creel and R. G. Barnes, *J. Chem. Phys.* **56**, 1549 (1972).

³¹R. B. Creel, S. L. Segel, R. J. Schoenberger, R. G. Barnes, and D. R. Torgeson, *J. Chem. Phys.* **60**, 2310 (1974).

³²C. Stassis, G. R. Kline, and S. K. Sinha, *Phys. Rev. Lett.* **31**, 1498 (1973).

³³S. Doniach and S. Engelsberg, *Phys. Rev. Lett.* **17**, 750 (1966).

³⁴T. Kasuya, in *Magnetism*, edited by G. T. Rado and H. Suhl (Academic, New York, 1966), Vol. II B, pp. 215–294.

³⁵W. E. Evenson and S. H. Liu, *Phys. Rev. Lett* **21**, 432 (1968).

³⁶W. E. Evenson, G. S. Fleming, and S. H. Liu, *Phys. Rev.* **178**, 930 (1969).

³⁷R. P. Gupta and S. K. Sinha, *Phys. Rev. B* **3**, 2401 (1971).

³⁸P. A. Fedders and P. C. Martin, *Phys. Rev.* **143**, 245 (1966).